CrossMark

Low-cost magnetic adsorbent for As(III) removal from water: adsorption kinetics and isotherms

Sarita Kango · Rajesh Kumar

Abstract Magnetite nanoparticles as adsorbent for arsenic (*As*) were coated on sand particles. The coated sand was used for the removal of highly toxic element 'As(III)' from drinking water. Here, batch experiments were performed with the variation of solution pH, adsorbent dose, contact time and initial arsenic concentration. The adsorbent showed significant removal efficiency around 99.6 % for As(III). Analysis of adsorption kinetics revealed that the adsorbent follows pseudo-second-order kinetics model showing $R^2 = 0.999$, whereas for pseudo-first-order kinetics model, the value of R^2 was 0.978. In the case of adsorption equilibrium, the data is well fitted with Langmuir adsorption isotherm model ($R^2 > 0.99$), indicating monolayer adsorption of As(III) on the surface of adsorbent. The existence of commonly present ions in water influences the removal efficiency of As(III) minutely in the following order $PO_4^{3-} > HCO_3^- > Cl^- > SO_4^{2-}$. The obtained adsorbent can be used to overcome the problem of water filtration in rural areas. Moreover, as the nano-magnetite is coated on the sand, it avoids the problem of extraction of nanoparticles from treated water and can easily be removed by a simple filtration process.

Keywords Sand · Magnetite nanoparticles · As(III) removal · Adsorption capacity · Kinetics · Isotherms

S. Kango · R. Kumar (✉)
Jaypee University of Information Technology, Waknaghat, Solan, Himachal Pradesh 173234, India
e-mail: rajesh.kumar@juit.ac.in

Introduction

Arsenic, a poisonous metalloid and a group 15 element, is a health wise dangerous contamination in both ground as well as in surface water. It has become a serious issue worldwide due to its negative impacts on human health and environment (Gu et al. 2005; Kanel et al. 2005; Desesso et al. 1998; Malana et al. 2011). The *As* contaminates water by weathering of arsenic-bearing rocks, volcanic action, forest fires, geochemical reactions, industrial wastewater discharge, agricultural uses of arsenical pesticides, herbicides, fertilizers, etc. (Jain and Ali 2000; Caussy 2003). Many parts of the world such as Bangladesh, West Bengal, India, and countries in South and Southeast Asia have shown massive epidemics of arsenic poisoning (Souter et al. 2003; Bagla and Kaiser 1996; Smith et al. 2000; Berg et al. 2001). The *As* toxicity and its hazardous effects on human health such as lung, kidney, bladder and skin cancers have been studied by a number of researchers (Kapas et al. 2006; Mazumdaer 2008; Jomova et al. 2011). Its exposure, even slightly higher than 0.1 mg/L in drinking water, may cause neurological damage, and its concentration reaching to 0.2 mg/L creates the problem of dermatosis (Chakraborti and Saha 1987). To avoid the problems caused by *As* contamination, the World Health Organization (WHO) and the United States Environmental Protection Agency (US EPA) have decreased its maximum concentration limit (MCL) from 50 to 10 μg/L (Caussy 2003; WHO 1993; Pena et al. 2006). For irrigation purposes, Food

and Agricultural Organization (FAO) has also set the same guideline value of *As*, i.e., 10 μg/L (FAO 1985).

Arsenic exists in the form of trivalent arsenite (as $H_3AsO_3^0$ and $H_2AsO_3^-$) and pentavalent arsenate (as $H_2AsO_4^-$ and $HAsO_4^{2-}$). The trivalent arsenite (As(III)) is 25 to 60 times more toxic than pentavalent arsenate (As(V)), and it is comparatively difficult to remove from water being nonionic at natural water pH (Raven et al. 1998; Bang et al. 2005; Kundu and Gupta 2007; Korte and Fernando 1991; Sarkar et al. 2005). There are many methods such as oxidation (Criscuoli et al. 2012), coagulation (Zouboulis and Katsoyiannis 2002), adsorption (Dhoble et al. 2011), ion exchange (Kim and Benjamin 2004), bioremediation (Cernansky et al. 2007) and membrane filtration (Zhao et al. 2012) suggested for *As* removal; however, most of them work only for the removal of less toxic As(V). Among these, the adsorption method can be adopted because both the As(III) and As(V) show strong affinity to iron-bearing substances such as goethite (Sun and Doner 1998), magnetite (Fe_3O_4) (Shipley et al. 2009), zero valent iron-reduced graphite oxide (Wang et al. 2014), ferrihydrite (Jessen et al. 2005), Mn-substituted Fe oxyhydroxide (Lakshmipathiraj et al. 2006), granular ferric hydroxide (Banerjee et al. 2008), Ce(IV)-doped Fe oxide (Zhang et al. 2003) and natural hematite and natural siderite (Guo et al. 2007). Iron oxide-based adsorption is most favourable for the adsorption of both the As(III) and As(V). If the iron-based adsorbent is made in nano-size, it will enhance the adsorption performance due to higher surface area as compared with bulk counterpart.

However, despite of having advantages, the iron-based nano-sized adsorbents have some limitations, for example, they need external magnetic field to be separated out from the water after use. A possible way to overcome the problem of requiring external magnetic field is that they can be used by making their filter cartridges, but again, this would be an expensive way since a large amount of the material would be needed in the cartridge. Therefore, the immobilization of the iron oxide nano-powder on an inexpensive material such as the sand would be a better way to pave the method to a cost effective technology. Among the iron oxides, magnetite (Fe_3O_4) shows high adsorption capacity and affinity (Shipley et al. 2009; Yean et al. 2005; Yavuz et al. 2006; An et al. 2011) to the *As*.

Here, we present a work to develop an inexpensive adsorbent by coating Fe_3O_4 nanoparticles on sand surface via co-precipitation method. The sand is used as a substrate for Fe_3O_4 to provide an economically feasible way for common man to get rid of the poisonous *As* from drinking water. Fe_3O_4-coated nano-adsorbent does not require any external magnetic field for the separation of the adsorbent. We have examined nano-magnetic adsorbent for the removal of As(III) from drinking water. In this study, batch experiments have been performed to analyse the influence of pH, adsorbent dose, initial As(III) concentration and contact time on the removal efficiency of As(III). The effect of commonly present ions (PO_4^{3-}, SO_4^{2-}, HCO_3^- and Cl^-) on the As(III) removal efficiency was also investigated. As an important concern, we have made the separation of nanosized Fe_3O_4 easier by avoiding the application of magnetic field. Here, by coating the nano-sized Fe_3O_4 adsorbent on the surface of sand particles, the filtration property of the sand has been used, which avoids the application of magnetic field for the separation of nano-sized Fe_3O_4. Moreover, the water filtration method being simple and low cost can be applied in the rural area to protect many lives.

Materials and methods

Materials

All the chemicals used in this study were of analytical grade, which were obtained from Sigma-Aldrich. The chemicals were used as received without further purification. The solutions used in this study were prepared in Milli-Q water. To prepare As(III) stock solution, a known amount of As(III) oxide was dissolved in Milli-Q water, and 4 g/L NaOH was used to enhance its solubility. To adjust the pH of solution, standard acid and base solutions 0.1 M HNO_3 and 0.1 M NaOH were used. Iron(III) chloride hexahydrate ($FeCl_3 \cdot 6H_2O$), iron(II) chloride ($FeCl_2$) and ammonia water (NH_4OH) were used for the synthesis of Fe_3O_4 nanoparticles. The substrate sand was cleaned and etched by hydrochloric acid (HCl) and aquaregia (HNO_3/HCl) solutions in 1:3 ratio, respectively. Potassium chloride (KCl) was used for determination of point of zero charge (pZ_{PZC}) of the adsorbent. We also studied ionic effect on the adsorption capacity of *As* by Fe_3O_4-coated sand, the ions were prepared using disodium hydrogen phosphate anhydrous (Na_2HPO_4), sodium sulphate (Na_2SO_4), sodium bicarbonate ($NaHCO_3$) and sodium chloride (NaCl)

salts which gave PO_4^{3-}, SO_4^{2-}, HCO_3^- and Cl^- ions in the solution.

Coating of Fe_3O_4 nanoparticles on sand surface

Fe_3O_4 nanoparticles coated sand was prepared using the procedure described earlier for iron-chitosan coating on sand with modification (Gupta et al. 2013). Initially, sand sieved to a geometric mean size of 0.6 to 0.9 mm was soaked in an acid solution (1.0 M HCl) for 24 h, which was then washed with distilled water several times and dried at 100 °C temperature. After cleaning, the sand was etched by using HNO_3/HCl in the ratio 1:3 for 5 min, and then, it was rinsed in a stream of water to remove the etchant solution. Thus, obtained sand was dispersed in a solution containing 2:1 ratio of $FeCl_3$ and $FeCl_2$, and NH_4OH solution was added drop wise at vigorous magnetic stirring keeping 70 °C temperature for 30 min under the flow of argon (Ar). The addition of NH_4OH led to the co-precipitation reaction and resulted in the formation of magnetite (Fe_3O_4) nanoparticles in the precursor solution. Since we added sand to the precursor solution, Fe_3O_4 nanoparticles were also nucleated on the surface of sand. The obtained mixture was aged at room temperature for 48 h, which was then filtered and dried in a furnace at 85 °C in the Ar gas environment. To ensure a proper coating of Fe_3O_4 nanoparticles on the surface of sand particles, the coated sand was washed with distilled water until a clear supernatant was obtained. After filtration, the sand was dried at 85 °C for 3 h. The Fe_3O_4 nanoparticles coated sand was stored in polyvinyl chloride (PVC) plastic bottles to perform batch experiments.

Determination of pH_{pzc} of the adsorbent

The pH_{pzc} of magnetite nanoparticles coated sand was also investigated in this study. For this, 0.1 M KCl solution was prepared and 25 mL of solution was taken in different flasks. The initial pH was adjusted between 2.0 and 12.0 by using 0.1 M NaOH and 0.1 M HCl. Then, 0.2 g of magnetite nanoparticles coated sand was added to each flask containing KCl solution of different pH. These flasks were kept on incubator shaker for 24 h, and the final pH of the solutions was measured and graphs were plotted between pH_{final} and $pH_{initial}$ (Sharma et al. 2009).

Batch adsorption experiments

In batch adsorption experiments, the parameters contact time, initial pH of aqueous solution, adsorbent dose and initial As(III) concentration were varied. All the experiments were performed at room temperature in an incubator shaker at an agitation speed of 200 rpm. To study the effect of contact time on As(III) adsorption, it was varied from 30 to 420 min, using 25 g/L Fe_3O_4 coated sand adsorbent at initial As(III) concentration of 1 mg/L, and pH 7.0. The pH of the solution was varied from 2.0 to 12.0 for fixed adsorbent dose, contact time 420 min, and initial As(III) concentrations of 1 mg/L at room temperature. The experiment of the adsorbent dose was performed by varying the dose from 5 to 30 g/L and keeping other parameters fixed. In the case of isotherm studies, the concentration of As(III) was varied from 3.5 to 103.8 mg/L for the fixed values of adsorbent dose, contact time and pH. Batch experiments were also performed to study the effect of prominent background ions viz. PO_4^{3-}, SO_4^{2-}, HCO_3^- and Cl^- on the As(III) removal efficiency. The concentration of these ions was varied from 5 to 100 mg/L, while other parameters were kept fixed. The solutions were first filtered using 0.45-μm durapore filter papers, then acidified with 1 % HNO_3, and finally analysed for residual As(III) concentration using inductively coupled plasma mass spectrometer (ICP-MS).

As(III) removal efficiency of Fe_3O_4 nanoparticles coated sand was calculated by using the formula:

$$\% \text{ As(III) removal} = \frac{C_0 - C_e}{C_0} \times 100 \qquad (1)$$

and the amount of As(III) adsorbed (mg) per unit mass of adsorbent (g), i.e., q_e, was determined by using the formula:

$$q_e = \frac{C_0 - C_e}{M} \times V \qquad (2)$$

where C_0 and C_e are initial and final As(III) concentrations (mg/L), respectively, V is the volume of solution in liters and M is the mass of the adsorbent in grams.

Desorption and readsorption experiment

Desorption studies for As(III) were carried out using 0.1- and 0.5-M sodium hydroxide solutions. Forty millilitres of 10 mg/L As(III) concentration was treated with 1 g of adsorbent for 7 h. The solution was filtered,

and the adsorbent was washed several times with distilled water to remove excess of unadsorbed As(III) ions. The saturated adsorbent was then treated with 40 ml of 0.1- and 0.5-M sodium hydroxide solutions separately for 7 h and then filtered and washed with distilled water to remove excess of sodium hydroxide. The adsorbent was again treated with 40 ml of As(III) solution of 10 mg/L to study the readsorption behaviour of the adsorbent.

Analytical measurements

To confirm the presence of Fe_3O_4 nanoparticles on the sand surface, X-ray diffraction (XRD) was performed by using XRD 6000, Shimadzu analytical instrument. Also, these nanoparticles were examined for morphology by Field Emission Scanning Electron Microscopy (FESEM), Hitachi S-4700. The initial and residual As(III) concentrations were determined by using ICP-MS, PerkinElmer Elan DRC 6000.

Results and discussion

Characterization of adsorbent

Figure 1 shows FESEM images of Fe_3O_4 nanoparticles, uncoated sand, and coated sand with Fe_3O_4 nanoparticles. From the reaction solution, some un-attached Fe_3O_4 nanoparticles were collected which are shown by SEM image in Fig. 1a. The nanoparticles have size

in the range of 20 to 60 nm. Figure 1b shows bare sand particles; it shows that before coating, the surface of the sand is clear, which after coating is covered with Fe_3O_4 nanoparticles of size 20 to 60 nm as shown in Fig. 1c, d. The FESEM images in Fig. 1a, d indicate that the Fe_3O_4 nanoparticles have the same morphology both in the solution as well as on the sand surface.

Figure 2 shows powder XRD patterns of Fe_3O_4 nanoparticles, uncoated sand, and Fe_3O_4 nanoparticles coated sand, respectively. In Fig. 2a, characteristic peaks at $2\theta = 30.1$, 35.5, 43.06, 53.04, 57.3 and 62.6° are consistent with Fe_3O_4 according to the JCPDS data (PDF No. 653107). In the XRD patter of coated sand (Fig. 2c), most of the peaks coincide with that of the pure Fe_3O_4 nanoparticles in Fig. 2a, indicating the formation of Fe_3O_4 nanoparticles on the surface of sand. In the case of uncoated sand, sharp and narrow peaks are obtained at different positions, which correspond to different faces present in sand, and also indicate high crystallinity of the sand as shown in Fig. 2b. Some of the peaks in the XRD pattern of the coated sand correspond to the peaks of uncoated sand.

Effect of contact time on As(III) removal: adsorption kinetics

Figure 3 shows the effect of contact time on % As(III) removal efficiency and adsorption capacity ($q_t = mg/g$) for initial As(III) concentration of 1 mg/L. We observed that the removal of As(III) takes place in two phases: In the first phase, the rapid removal (82.84 % of As(III)

Fig. 1 FESEM image of **a** Fe_3O_4 nanoparticles, **b** uncoated sand and **c, d** Fe_3O_4 nanoparticles coated on sand surface
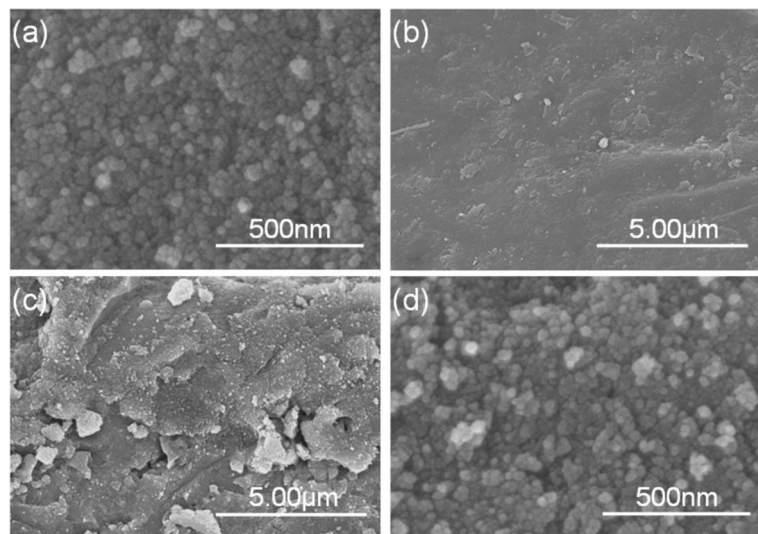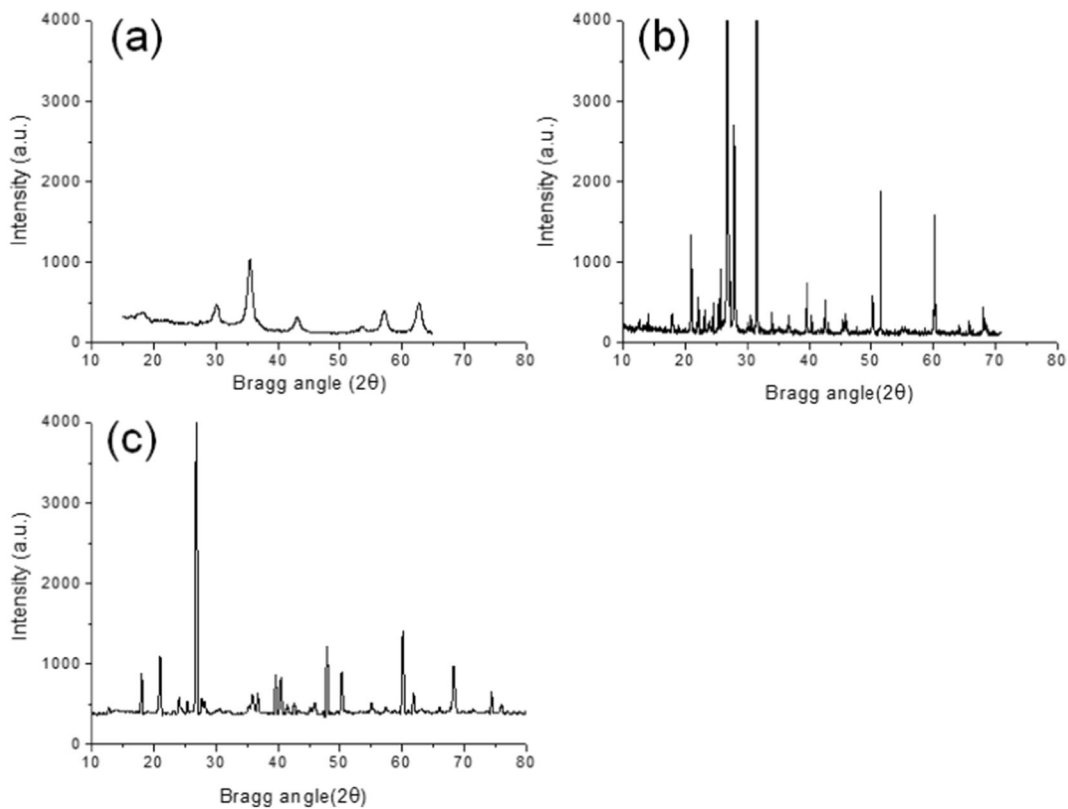
Fig. 2 XRD pattern of **a** Fe_3O_4 nanoparticles, **b** uncoated sand and **c** Fe_3O_4 nanoparticles coated sand

was removed) takes place within initial 30 min of contact time, and in the second phase, the removal rate decreases and takes about 360 min to achieve adsorption equilibrium as shown in Fig. 3. However, the adsorption equilibrium was achieved in about 360 min, but to ensure complete adsorption, we performed all the batch experiments for prolonged contact time, i.e., 420 min. The observed fast adsorption of As(III) by Fe_3O_4

Fig. 3 Effect of contact time on % As(III) removal efficiency and adsorption capacity ($q_t = mg/g$)

nanoparticles coated sand in the first phase is due to an external surface adsorption process. In this process, all the adsorption sites existing on the external surface are occupied at a fast rate by adsorbing As(III) (in our case 30 min). Adsorption mechanism occurred in the first phase can be termed as 'adsorption controlled by the surface process' (Chowdhury and Yanful 2010). After 30 min, when all the external adsorption sites of Fe_3O_4 are filled, the process of *As* removal becomes slower because the As(III) do not find an immediate contact surface in the Fe_3O_4 nanoparticles; however, the sub-layered Fe_3O_4 nanoparticles would still have adsorption sites for *As* adsorption. Once the external adsorption sites are occupied, the As(III) approaches to the available adsorption sites on the surface of sub-layered Fe_3O_4 nanoparticles. In this process, to reach the available adsorption sites, the As(III) has to diffuse through the Fe_3O_4 nanoparticles. Due to the inter-particle diffusion of As(III), the rate of adsorption decreases. Since the process is now diffusion controlled, therefore it can be termed as 'adsorption controlled by diffusion' (Ren et al. 2011). Here, we can say that longer is the inter-particle diffusion distance slower the adsorption rate is.
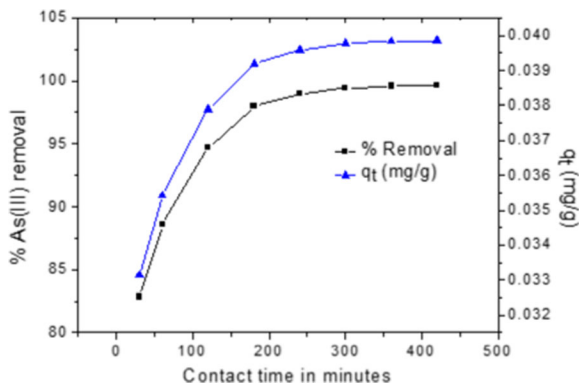
At equilibrium, 99.60 % As(III) was removed for an initial As(III) concentration of 1 mg/L.

To estimate the rate of adsorption and rate controlling step, pseudo-first-order and pseudo-second-order kinetics model were employed. Following Eq. (3) represents pseudo-first-order kinetics model (Lagergren 1898).

$$\log(q_e - q_t) = \log q_e - \frac{k_{ads}}{2.303}t \qquad (3)$$

where q_e (mg/g) and q_t (mg/g) are amount of As(III) adsorbed per unit mass of adsorbent at equilibrium and at time t, respectively. The k_{ads} is pseudo-first-order rate constant, which can be obtained from slope of linear plot log (q_e-q_t) vs time (t).

Similarly, Eq. (4) represents pseudo-second-order kinetics model (Ho and McKay 1998).

$$\frac{t}{q_t} = \frac{1}{h} + \frac{t}{q_e} \qquad (4)$$

and

$$h = kq_e^2 \qquad (5)$$

where q_e (mg/g) and q_t (mg/g) are amount of As(III) adsorbed per unit mass of adsorbent at equilibrium and at time t, respectively. Here, k is pseudo-second-order adsorption rate constant, and h is initial adsorption rate (mg g^{-1} h^{-1}). The values of q_e (1/slope), k (slope^2/intercept) and h (1/intercept) can be calculated from the plots of t/q_t vs t. The plots of pseudo-first-order and pseudo-second-order kinetics model are shown in Fig. 4a, b, respectively. The values of various corresponding parameters viz. k_{ads}, k, h and correlation coefficients R^2 obtained from these plots are shown in Table 1. The experimental data is fitted well in the pseudo-second-order kinetics model with higher correlation coefficient ($R^2 = 0.999$) as compared with pseudo-first-order kinetics model with correlation coefficient $R^2 = 0.978$. Also, the experimental value of q_e (0.0398) is more close to the theoretical value (0.040) of q_e obtained from pseudo-second-order model as compared to q_e (0.015) obtained from pseudo-first-order-model. This reveals that adsorption process is chemisorption, i.e., there exists some chemical bonding between adsorbent and adsorbate (Ren et al. 2011).

Intra-particle diffusion model was also used to explain the adsorption mechanism. Equation (6) represents intra-particle diffusion model (Weber and Morris 1963).

$$q_t = k_i t^{1/2} \qquad (6)$$

where k_i is intra-particle diffusion rate constant and q_t is the amount of As(III) adsorbed per unit mass of adsorbent at time t. The plot of intra-particle diffusion model is shown in Fig. 5. Values of intra-particle diffusion rate constant obtained from the slope of the plot and correlation coefficient (R^2) are given in Table 1. According to this model, if the graph between q_t and $t^{1/2}$ gives a straight line then intra-particle diffusion is the rate-limiting step. Further, it is also essential that the plot should pass through the origin for intra-particle diffusion to be the sole rate limiting step.

However, in the present study, the plot of q_t and $t^{1/2}$ is not a straight line, and also, the plot does not pass through the origin as indicated in Fig. 5. It is clear from the Fig. 5 that three steps are involved in the adsorption process: (i) sharper portion attributes boundary layer diffusion of solute molecules, (ii) second portion indicates a gradual adsorption phase, where intra-particle
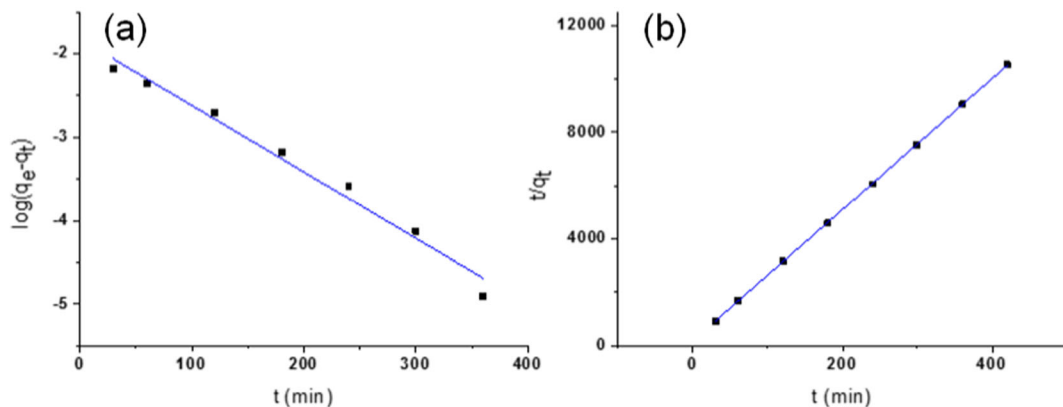

Fig. 4 Adsorption kinetics, **a** pseudo-first-order model and **b** pseudo-second-order model for As(III) removal by Fe$_3$O$_4$ nanoparticles coated sand

Table 1 Pseudo-first-order and pseudo-second-order kinetic parameters, and intra-particle diffusion model parameters for As(III) adsorption by Fe_3O_4 nanoparticles coated sand

Pseudo-first-order parameters			Pseudo-second-order parameters					Experimental q_e (mg/g)	Intra-particle diffusion model parameters	
k_{ads} (min^{-1})	R^2	q_e	k (g mg^{-1} min^{-1})	h (mg g^{-1} min^{-1})	q_e (mg g^{-1})	R^2			K_i (mg g^{-1} min$^{1/2}$)	R^2
0.0183	0.978	0.015	3.21	0.0053	0.040	0.999		0.0398	0.000432	0.824

diffusion is rate limiting step followed, and (iii) final equilibrium phase.

Effect of solution pH on the removal of As(III)

The pH of water is considered an important factor in the adsorption-based wastewater treatment experiments (Escudero et al. 2009) as it affects metal speciation in the water. Figure 6 shows the effect of water pH on the removal efficiency and adsorption capacity of As(III) by Fe_3O_4 coated sand. The effect of pH can be explained in terms of pH_{pzc} of the adsorbent (pH_{pzc} of adsorbent is nearly 7.8, represented by the intersection point of the plots in Fig. 7) at which the surface of the adsorbent is neutral. From Fig. 6, it can be seen that with an increase in the pH of water from 2.0 to 8.0, As(III) removal efficiency increases from 98.92 to 99.63 %, and the adsorption capacity increases from 0.0395 to 0.0398 mg/g. This is due to the fact that below pH_{pzc} (7.8), the surface of adsorbent Fe_3O_4 is positively charged and As(III) exists in nonionic (H_3AsO_3) state in the low pH (2.0 to 6.0) range. Therefore, when nonionic As(III) species comes in contact with Fe_3O_4 its positively charged surface helps nonionic As(III) to convert into anionic one, which in turn assists

adsorption process (Gupta et al. 2013; Kundu and Gupta 2006). At pH values 6.5 to 8.0, the neutral As(III) ions dissociate and produce anionic $H_2AsO_3^{-1}$ and $HAsO_3^{-2}$ ions which are attracted to positively charged surface (below pH 7.8) of adsorbent resulting in high As(III) removal.

Even in the pH range from 8.0 to 12.0, As(III) remains in anionic state, but above pH_{pzc} (7.8), the adsorbent surface become negatively charged. Therefore, in this pH range, the decreasing As(III) uptake from 99.63 to 62.8 % and decreasing adsorption capacity from 0.0398 to 0.0251 mg/g are due the following reasons: (i) the competition of excessive OH^- ions for adsorption, (ii) domination of negatively charged sites on Fe_3O_4 nanoparticles coated sand and (iii) domination of negatively charged As(III) species ($H_2AsO_3^-$). With increasing pH, there is a gradual increase in the repulsive forces between negatively charged Fe_3O_4 nanoparticles coated sand and the negatively charged As(III) ions, which results in a decreasing As(III) removal efficiency (Ranjan et al. 2009; Dhoble et al. 2011; Dhoble et al. 2012). We know that most of the groundwater exists in the pH range from 7.0 to 7.5; therefore, in this study, we have analysed batch experiments at most natural pH '7.0'.
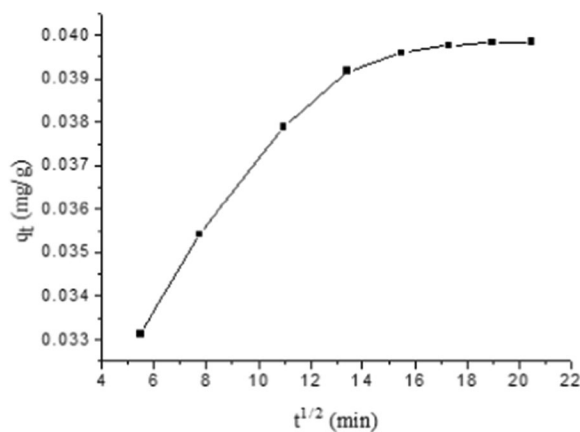

Fig. 5 Intra-particle diffusion model for As(III) removal by Fe_3O_4 nanoparticles coated sand
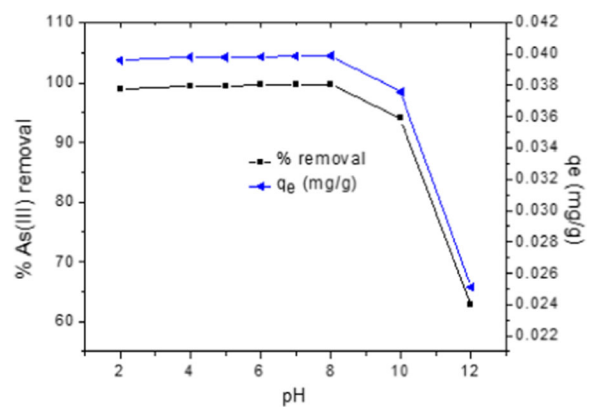

Fig. 6 Effect of pH on % As(III) removal efficiency and adsorption capacity (q_e = mg/g)
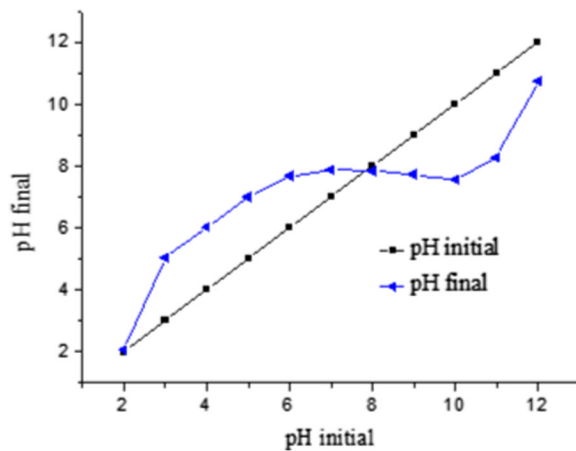
Fig. 7 pH initial versus pH final plot for the determination of pH$_{pzc}$ of adsorbent

Effect of adsorbent dose

Figure 8 shows the effect of adsorbent dose on % As(III) removal efficiency and adsorption capacity (q_e = mg/g) at fixed initial As(III) concentration '1 mg/L', and pH '7.0'. It was observed that with an increase in the adsorbent dose from 5 to 30 g/L, the As(III) removal efficiency increased from 88.93 to 99.89 %, which occurs due to available more active sites at higher concentrations of the adsorbent (Pandey et al. 2009; Kaczala et al. 2009). In fact, beyond 25 g/L of dose, there was no significant change in As(III) removal efficiency. On the other hand, the adsorption capacity decreased from 0.178 to 0.0333 mg/g. This decrease is deduced from the interference between binding sites, and higher adsorbent dose or inadequate number of *As* ions in the solution with respect to available binding sites (Fan et al. 2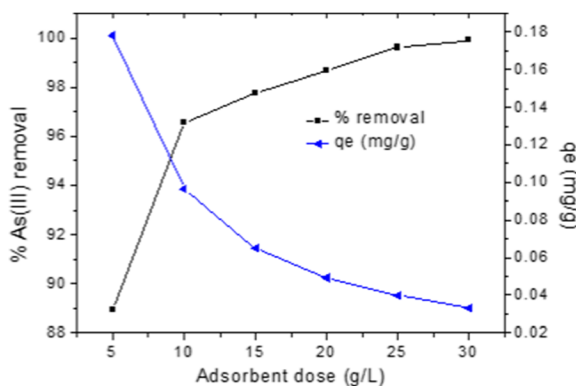008; Rome and Gadd 1987). In this plot, the point of intersection (Fig. 8) is usually considered as the optimum dose that represents balance between % As(III) removal and adsorption capacity. In our case, the point of intersection is approximately at 10 g/L of adsorbent dose, but for this dose, only 96.55 % As(III) removal was achieved, and 0.0344 mg/L As(III) was still there in the solution, which is higher than the MCL value set by WHO. Therefore, a dose of 25 g/L, at which *As* level dropped below the MCL value, was selected for further analysis. Importantly, in this study, it should be noted that the dose of real adsorbent (Fe$_3$O$_4$ nanoparticles) would be much smaller than the weighted dose as the weighted dose includes bulky sand particles as well. In other words, the weighted dose is the combination of real adsorbent, i.e., Fe$_3$O$_4$ nanoparticles and the sand particles.

Effect of initial As(III) concentration

Figure 9 shows the effect of initial As(III) concentration on the removal efficiency and adsorption capacity of Fe$_3$O$_4$ nanoparticles coated sand. It is observed that with the increase in initial As(III) concentration, the As(III) removal efficiency decreases, while the adsorption capacity increases and became saturated at 80 mg/L of As(III) concentration, and further addition of As(III) does not cause significant change in adsorption capacity. This is because at lower As(III) concentration, the number of adsorbent surface active sites is sufficiently large and accommodates abundant of As(III) ions. An increase in the As(III) concentration causes a reduction in the proportion of surface active sites to As(III) ions, and thus an insufficient accommodation of As(III) ions results in the decreasing % As(III) removal efficiency.
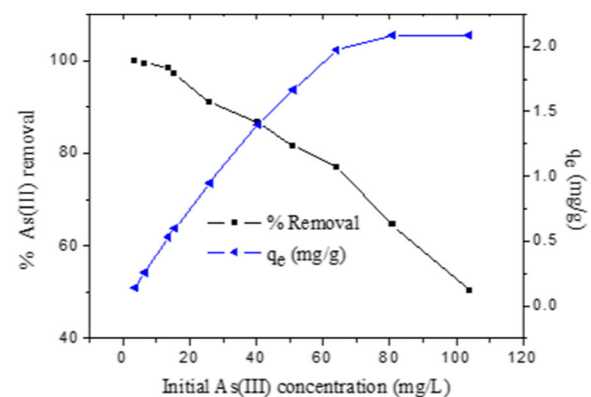

Fig. 8 Effect of adsorbent dose on % As(III) removal efficiency and adsorption capacity (q_e = mg/g)

Fig. 9 Effect of initial As(III) concentration on % As(III) removal efficiency and adsorption capacity (q_e = mg/g)
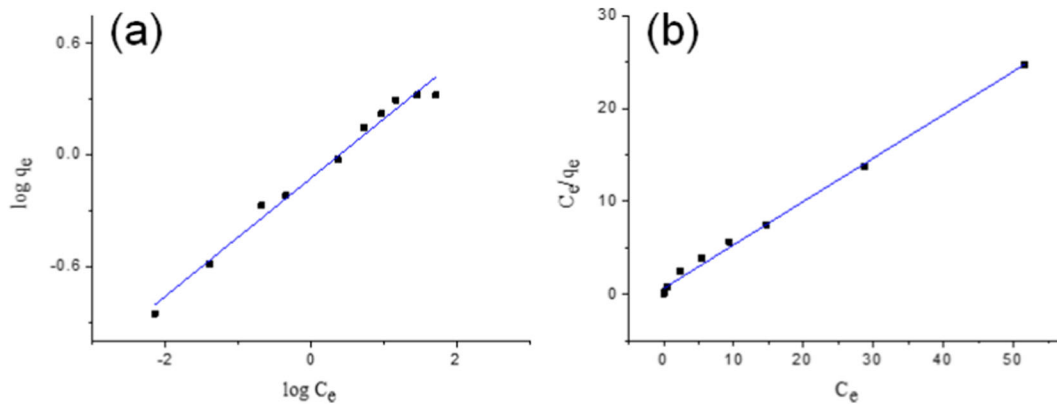
Fig. 10 Adsorption isotherm, **a** Freundlich fit and **b** Langmuir fit for As(III) adsorption by Fe_3O_4 nanoparticles coated sand

Furthermore, a driving force is provided by initial As(III) concentration to overcome all mass transfer resistances between the adsorbent and adsorption medium which results in higher adsorption capacities at higher initial As(III) concentration (Fan et al. 2008).

Adsorption isotherms

We know that the adsorption isotherm gives an idea about the interaction between adsorbate and adsorbent in an adsorption system. Therefore, in order to study the adsorbate-adsorbent interaction, and to compute various adsorption parameters, we have used Freundlich and Langmuir isotherm models to fit the adsorption equilibrium data of As(III) on Fe_3O_4 nanoparticles coated sand. The Freundlich isotherm in linear form is represented as (Freundlich 1906)

$$\log(q_e) = \log K_F + \frac{1}{n}\log(C_e) \qquad (7)$$

where C_e is the equilibrium concentration of As(III) in solution phase(mg/L), q_e is the amount of As(III) adsorbed onto the Fe_3O_4 nanoparticles coated sand at equilibrium (mg/g), K_F is adsorption capacity indicator and n (which lies between 1 to 10) is the heterogeneity factor indicating favourable adsorption. It is reported that if the value of n lies between 2 to 10, the adsorption is considered as better adsorption, and if it lies between 1 to 2, the adsorption is considered to be good.

Linear form of Langmuir isotherm model can be written as (Wang et al. 2012)

$$\frac{C_e}{q_e} = \frac{C_e}{q_m} + bq_m \qquad (8)$$

where C_e and q_e are the As(III) concentration in the solution and As(III) amount adsorbed at equilibrium, respectively. The q_m (mg/g) is saturated monolayer adsorption capacity, and b (L/mg) is Langmuir constant related to the affinity between solute and adsorbent.

A dimensionless quantity 'r' was also calculated in order to predict the adsorption efficiency of the process by using following equation.

$$r = \frac{1}{1 + bC_0} \qquad (9)$$

where C_0 is the initial concentration of As(III) and b is the Langmuir constant. Value of r less than 1.0 represents favourable adsorption, whereas r greater than 1.0 represents unfavourable adsorption. For Fe_3O_4 nanoparticles coated sand adsorbent, Linearized Freundlich and Langmuir adsorption isotherm plots are shown in Fig. 10a, b, respectively. Values corresponding to various parameters of Langmuir and Freundlich isotherms are listed in Table 2.

In our case, the calculated value of n is 3.15, which lies between the limit of better adsorption, i.e., $2 < n < 10$ of As(III) on Fe_3O_4 nanoparticles coated sand. The obtained higher correlation coefficient ($R^2 > 0.99$) while using Langmuir model indicates that the experimental data are better fitted by Langmuir model as compared with Freundlich model where R^2 is smaller than the previous one. This interprets monolayer adsorption of As(III) on a homogeneous surface. Here, the maximum adsorption capacity (K_F) for As(III) removal is obtained 2.14 mg/g, which is comparable with other reported adsorbents. The comparison of Freundlich adsorption

Table 2 Freundlich and Langmuir adsorption isotherm parameters for As(III) adsorption by Fe_3O_4 nanoparticles coated sand

Freundlich isotherm parameters			Langmuir isotherm parameters			
K_F (mg/g)	n	R^2	b (L/mg)	q_m(mg/g)	R	R^2
0.75	3.15	0.983	0.709	2.14	0.287–0.013	0.996

capacity of Fe_3O_4 nanoparticles coated sand for As(III) removal with reported low-cost adsorbents is given in Table 3. The value of r is obtained to be less than unity with a decreasing order at high As(III) concentrations, which indicates highly favourable adsorption of As(III) on Fe_3O_4 nanoparticles coated sand.

Effect of background ions on As(III) removal efficiency

The ions such as PO_4^{3-}, SO_4^{2-}, HCO_3^- and Cl^- are commonly present in water and may affect the adsorption efficiency of any adsorbent. Considering this

fact, we have studied their influence on the As(III) removal efficiency. Figure 11 shows the results for individual effects of various background ions (PO_4^{3-}, SO_4^{2-}, HCO_3^- and Cl^-) on % As(III) removal efficiency by Fe_3O_4 nanoparticles coated sand. Here, the presence of sulphate shows a negligible effect on the As(III) removal efficiency, whereas the other ions Cl^-, HCO_3^- and PO_4^{3-} have bit more influence, but it is still minute for their concentration range from 5 to 100 mg/L.

The presence of these anions having little to no effect on As(III) removal efficiency may be attributed to the type of complex formed between the surface of Fe_3O_4 nanoparticles coated sand and As(III) ions (Luther et al. 2012). Although it is well known that PO_4^{3-} effects the removal of *As*, but in this study, we observed that the presence of PO_4^{3-} shows a minute influences on the removal of *As* by Fe_3O_4 nanoparticles coated sand. The reason for this minute effect can be inferred as that there is formation of iron(III) phosphate, which removes As(III) through oxidation followed by subsequent exchange of As(V) with PO_4^{3-} ions (Lenoble et al. 2005). The effect co-existing ions on the As(III) removal efficiency is in the order $PO_4^{3-} > HCO_3^- > Cl^- > SO_4^{2-}$, which is shown in Fig. 10.

Table 3 Comparative account of adsorption capacities of some adsorbents for As(III) removal

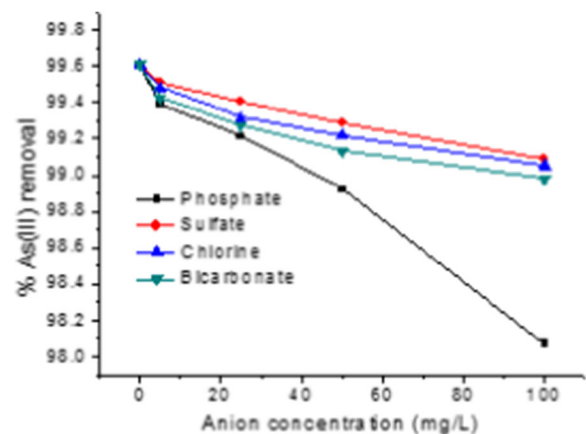| Low cost adsorbents	Langmuir adsorption capacity q_m (mg/g)	References
Iron oxide coated sand	0.029	(Gupta et al. 2005)
Iron acetate coated activated alumina	0.090	(Das et al. 2013)
China clay and fly ash	0.389	(Singh et al. 2009)
Iron-manganese oxide coated sand	0.55	(Lekic et al. 2013)
Manganese oxide minerals	0.676	(Ergül et al. 2014)
Blast furnace slag	0.70	(Lekic et al. 2013)
Iron oxide impregnated activated alumina	0.734	(Kuriakose et al. 2004)
Modified blast furnace slag	0.82	(Lekic et al. 2013)
Shale sedimentary rock	0.987	(Yusof et al. 2009)
TiO_2 nanoparticles	1.6	(Danish et al. 2013)
Ag-TiO_2 nanoparticles	1.71	(Danish et al. 2013)
Fe-TiO_2 nanoparticles	3.08	(Danish et al. 2013)
Fe_3O_4 nanoparticles coated sand	2.14	Present study

Fig. 11 Effect of co-existing anions on As(III) removal efficiency

Table 4 Desorption data for As(III) adsorbed on magnetite nanoparticles coated sand using different concentrations of sodium hydroxide

Concentration of As(III) (mg/L)	Removal efficiency (%)	Desorption (%) with NaOH	
		0.1 M	0.5 M
10	98.73	65.5	76.33

Desorption and readsorption efficiency of adsorbent

The desorption data for As(III) adsorbed on magnetite nanoparticles coated sand using different concentrations of sodium hydroxide is shown in Table 4. It has been observed that with 0.1 M NaOH solution, 65.5 % of As(III) was desorbed from the adsorbent, and with increase in NaOH concentration to 0.5 M, 76.33 % of As(III) was desorbed. In readsorption experiment, it was found that 58.33 and 65.65 % of As(III) was readsorbed by adsorbent treated with 0.1 and 0.5 M NaOH, respectively.

In Fig. 12, we demonstrate the proposed mechanism for adsorption of As(III) species (H_3AsO_3, $H_2AsO_3^-$ and $HAsO_3^{2-}$) on Fe_3O_4 nanoparticles coated sand particle.

Conclusions

Fe_3O_4 nano-adsorbent has been coated successfully on the surface of sand particles. The kinetic study shows that the equilibrium is reached within 360 min and fitted well with pseudo-second-order kinetics model rather than pseudo-first-order kinetics model. Adsorption isotherm data is well fitted in Langmuir adsorption isotherm with higher correlation coefficient ($R^2 > 0.99$). The obtained adsorbent shows a significant '99.6 %' of As(III) removal in most natural conditions. The Fe_3O_4 shows high adsorption capacity and affinity toward *As* thus by utilizing the Fe_3O_4 coated sand in the filter assembly the problem of external magnetic field can be eliminated. Moreover, the nano-adsorbent
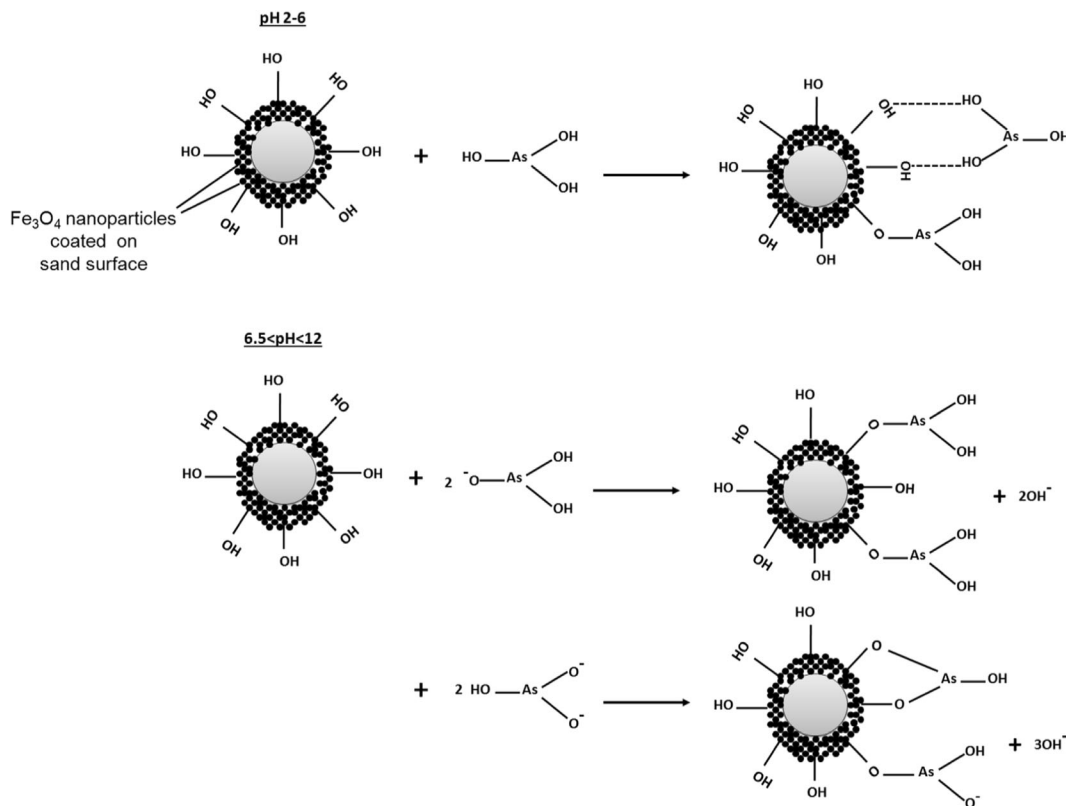

Fig. 12 Schematic diagram for As(III) adsorption mechanism by Fe_3O_4 nanoparticles coated sand particle

'Fe$_3$O$_4$' coated sand provides an economical and feasible method for a common man to remove As(III) from drinking water.

References

An, B., Liang, Q., & Zhao, D. (2011). Removal of arsenic (V) from spent ion exchange brine using a new class of starch-bridged magnetite nanoparticles. *Water Research, 45*(5), 1961–1972.

Bagla, P., & Kaiser, J. (1996). India's spreading health crisis draws global arsenic experts. *Science, 274*(5285), 174–175.

Banerjee, K., Amy, G. L., Prevost, M., Nour, S., Jekel, M., Gallagher, P. M., & Blumenschein, C. D. (2008). Kinetic and thermodynamic aspects of adsorption of arsenic onto granular ferric hydroxide (GFH). *Water Research, 42*(13), 3371–3378.

Bang, S., Johnson, M. D., Korfiatis, G. P., & Meng, X. (2005). Chemical reactions between arsenic and zero-valent iron in water. *Water Research, 39*(5), 763–770.

Berg, M., Tran, H. C., Nguyen, T. C., Pham, H. V., Schertenleib, R., & Giger, W. (2001). Arsenic contamination of groundwater and drinking water in Vietnam: a human health threat. *Environmental Science and Technology, 35*(13), 2621–2626.

Caussy, D. (2003). Case studies of the impact of understanding bioavailability: arsenic. *Ecotoxicology and Environmental Safety, 56*(1), 164–173.

Cernansky, S., Urik, M., Sevc, J., & Khun, M. (2007). Biosorption and biovolatilization of arsenic by heat-resistant fungi. *Environmental Science and Pollution Research, 14*(1), 31–35.

Chakraborti, A. K., & Saha, K. C. (1987). Arsenical dermatosis from tube well water in West Bengal. *Indian Journal of Medical Research, 85*, 326–334.

Chowdhury, S. R., & Yanful, E. K. (2010). Arsenic and chromium removal by mixed magnetite-maghemite nanoparticles and the effect of phosphate on removal. *Journal of Environmental Management, 91*(11), 2238–2247.

Criscuoli, A., Majumdar, S., Figoli, a., Sahoo, G. C., Bafaro, P., Bandyopadhyay, S., & Drioli, E. (2012). As(III) oxidation by MnO$_2$ coated PEEK-WC nanostructured capsules. *Journal of Hazardous materials, 211-212*, 281–287.

Danish, M. I., Qazi, I. A., Zeb, A., Habib, A., Awan, M. A., & Khan, Z. (2013). Arsenic removal from aqueous solution using pure and metal-doped titania nanoparticles coated on glass beads: adsorption and column studies. *Journal of Nanomaterials, 2013*(2013), 1–17.

Das, B., Devi, R. R., Umlong, I. M., Borah, K., Banerjee, S., & Talukdar, A. K. (2013). Arsenic (III) adsorption on iron acetate coated activated alumina: thermodynamic, kinetics and equilibrium approach. *Journal of Environmental Health Science and Engineering, 11*(42), 1–10.

Desesso, J. M., Jacobson, C. F., Scialli, A. R., Farr, C. H., & Holson, J. F. (1998). An assessment of the developmental toxicity of inorganic arsenic. *Reproductive Toxicology, 12*(4), 385–433.

Dhoble, R. M., Lunge, S., Bhole, A. G., & Rayalu, S. (2011). Magnetic binary oxide particles (MBOP): a promising adsorbent for removal of As(III) in water. *Water Research, 45*(16), 4769–4781.

Dhoble, R. M., Lungea, S., Bhole, A. G., & Rayalu, S. (2012). *Low cost magnetic iron oxide (MIO) adsorbent potential for arsenic removal* (pp. 271–275). Dubai: International conference on chemical, civil and environment engineering. March 24-25.

Ergül, B., Bektaş, N., & Öncel, M. S. (2014). The use of manganese oxide minerals for the removal arsenic and selenium anions from aqueous solutions. *Energy and Environmental Engineering, 2*(5), 103–112.

Escudero, C., Fiol, N., Villaescusa, I., & Bollinger, J. C. (2009). Arsenic removal by waste metal (hydr)oxide entrapped into calcium alginate beads. *Journal of Hazardous materials, 164*(2-3), 533–541.

Fan, T., Liu, Y., Feng, B., Zeng, G., Yang, C., Zhou, M., Zhou, H., Tan, Z., & Wang, X. (2008). Biosorption of cadmium(II), zinc(II) and lead(II) by *Penicillium simplicissimum*: isotherms, kinetics and thermodynamics. *Journal of Hazardous materials, 160*(2-3), 655–661.

FAO, (1985). Water quality guidelines for maximum crop production. Food and Agriculture Organization/UN, <http://www.fao.org/docrep/T0551E>(13.9.06)

Freundlich, H. M. F. Z. (1906). Stoechiometrie und Verwandtschaftslehre. *Zeitschriftfuer Physikalische Chemie, 57*, 385–470.

Gu, Z. M., Fang, J., & Deng, B. L. (2005). Preparation and evaluation of GAC-based iron-containing adsorbents for arsenic removal. *Environmental Science and Technology, 39*(10), 3833–3843.

Guo, H. M., Stuben, D., & Berner, Z. (2007). Adsorption of arsenic (III) and arsenic(V) from groundwater using natural siderite as the adsorbent. *Journal of Colloid and Interface Science, 315*(1), 47–53.

Gupta, A., Mohammed, Y., & Sankararmakrishnan, N. (2013). Chitosan- and Iron- chitosan-coated sand filters: a cost-effective approach for enhanced arsenic removal. *Industrial and Engineering Chemistry Research, 52*(5), 2066–2072.

Gupta, V. K., Saini, V. K., & Jain, N. (2005). Adsorption of As(III) from aqueous solutions by iron oxide-coated sand. *Journal of Colloid and Interface Science, 288*, 55–60.

Ho, Y. S., & McKay, G. (1998). Kinetic models for the sorption of dye from aqueous solution by wood. *Journal of Environmental Science and Health Part B: Process Safety Environmental Protection, 76*(2), 183–191.

Jain, C. K., & Ali, I. (2000). Arsenic: occurrence, toxicity and speciation techniques. *Water Research, 34*(17), 4304–4312.

Jessen, S., Larsen, F., Koch, C. B., & Avin, E. (2005). Sorption and desorption of arsenic to ferrihydrite in a sand filter. *Environmental Science and Technology, 39*(20), 8045–8051.

Jomova, K., Jenisova, Z., Feszterova, M., Baros, S., Liska, J., Hudecova, D., Rhodes, C. J., & Valko, M. (2011). Arsenic:

toxicity, oxidative stress and human disease. *Journal of Applied Toxicology, 31*(2), 95–107.

Kaczala, F., Marques, M., & Hogland, W. (2009). Lead and vanadium removal from a real industrial wastewater by gravitational settling/sedimentation and sorption onto *Pinus sylvestris* sawdust. *Bioresource Technology, 100*(1), 235–243.

Kanel, S. R., Manning, B., Charlet, L., & Choi, H. (2005). Removal of arsenic(III) from groundwater by Nanoscale zero-valent iron. *Environmental Science and Technology, 39*(5), 1291–1298.

Kapas, S., Peterson, H., Liber, K., & Bhattacharya, P. (2006). Human health effects from chronic arsenic poisoning- a review. *Journal of Environmental Science and Health, Part A: Toxic/Hazardous Substances and Environmental Engineering, 41*(10), 2399–2428.

Kim, J., & Benjamin, M. M. (2004). Modeling a novel ion exchange process for arsenic and nitrate removal. *Water Research, 38*(8), 2053–2062.

Korte, N. E., & Fernando, Q. (1991). A review of As(III) in groundwater. *Critical Reviews in Environmental Control, 21*(1), 1–39.

Kundu, S., & Gupta, A. K. (2006). Adsorptive removal of As(III) from aqueous solution using iron oxide coated cement (IOCC): evaluation of kinetics, equilibrium and thermodynamic models. *Separation and Purification Technology, 51*(2), 165–172.

Kundu, S., & Gupta, A. K. (2007). As(III) removal from aqueous medium in fixed bed using iron oxide-coated cement (IOCC): experimental and modeling studies. *Chemical Engineering Journal, 129*(1-3), 123–131.

Kuriakose, S., Singh, T. S., & Pant, K. K. (2004). Adsorption of As(III) from aqueous solution onto iron oxide impregnated activated alumina. *Water Quality Research Journal Canada, 39*(3), 258–266.

Lagergren, S. (1898). About the theory of so-called adsorption of soluble substance. *Kungliga Svenska Vetenskapsakademiens Handlingar, 24*, 1–39.

Lakshmipathiraj, P., Narasimhan, B. R. V., Prabhakar, S., & Bhaskar, R. G. (2006). Adsorption studies of arsenic on Mn-substituted iron oxyhydroxide. *Journal of Colloid and Interface Science, 304*(2), 317–322.

Lekic, B. M., Markovic, D. D., Rajakovic-Ognjanovic, V. N., Yukic, A. R., & Rajakovic, L. V. (2013). Arsenic removal from water using industrial by-products. *Journal of Chemistry, 2013*, 121024(1)–121024(9).

Lenoble, C., Laclautre, V., Deluchat, B. S., & Bollinger, J. C. (2005). Arsenic removal by adsorption on iron (III) phosphate. *Journal of Hazardous materials, 123*(1-3), 262–268.

Luther, S., Borgfeld, N., Kim, J., & Parsons, J. G. (2012). Removal of arsenic from aqueous solution: a study of the effects of pH and interfering ions using iron oxide nanomaterials. *Michrochemical Journal, 101*(2012), 30–36.

Malana, M. A., Qureshi, R. B., & Ashiq, M. N. (2011). Adsorption studies of arsenic on nano aluminium doped manganese copper ferrite polymer (MA, VA, AA) composite: kinetics and mechanism. *Chemical Engineering Journal, 172*(2-3), 721–727.

Mazumdaer, D. N. G. (2008). Chronic arsenic toxicity and human health. *Indian Journal of Medical Research, 128*(4), 436–447.

Pandey, P. K., Choubey, S., Verma, Y., Pandey, M., & Chandrashekhar, K. (2009). Biosorptive removal of arsenic from drinking water. *Bioresource Technology, 100*(2), 634–637.

Pena, M. E., Meng, X. G., Korfiatis, G. P., & Jing, C. Y. (2006). Adsorption mechanism of arsenic on nanocrystalline titanium dioxide. *Environmental Science and Technology, 40*(4), 1257–1262.

Ranjan, D., Talat, M., & Hasan, S. H. (2009). Biosorption of arsenic from aqueous solution using agriculture residue rice polish. *Journal of Hazardous materials, 166*(2-3), 1050–1059.

Raven, K. P., Jain, A., & Loeppert, R. H. (1998). Arsenite and arsenate adsorption on ferrihydrite: kinetics, equilibrium, and adsorption envelope. *Environmental Science and Technology, 32*(3), 344–349.

Ren, Z., Zhang, G., & Chen, J. P. (2011). Adsorptive removal of arsenic from water by an iron-zirconium binary oxide adsorbent. *Journal of Colloid and Interface Science, 358*(1), 230–237.

Rome, L., & Gadd, G. M. (1987). Copper adsorption by *Rhizopus arrhizus*, *Cladosorium resinae* and *Penicillium italicum*. *Applied Microbiology and Biotechnology, 26*(1), 84–90.

Sarkar, S., Gupta, A., Biswas, R. K., Deb, A. K., Greenleaf, J. E., & Sen Gupta, A. K. (2005). Well head arsenic removal units in remote villages in Indian Subcontinent: field results and performance evaluation. *Water Research, 39*(10), 2196–2206.

Sharma, Y. C., Uma, S., & Upadhyay, S. N. (2009). Removal of a cationic dye from wastewaters by adsorption on activated carbon developed from coconut coir. *Energy and Fuels, 23*, 2983–2988.

Shipley, H. J., Yean, S., Kan, A. T., & Tomson, M. B. (2009). Adsorption of arsenic to magnetite nanoparticles: effect of particle concentration, pH, ionic strength, and temperature. *Environmental Toxicology and Chemistry, 28*(3), 509–515.

Singh, A. P., Srivastava, K. K., & Shekhar, H. (2009). Arsenic (III) removal from aqueous solutions by mixed adsorbent. *Indian Journal of Chemical Technology, 16*, 136–141.

Smith, A. H., Lingas, E. O., & Rahman, M. (2000). Contamination of drinking-water by arsenic in Bangladesh: a public health emergency. *Bulletin of the World Health Organization, 78*(9), 1093–1103.

Souter, P. F., Cruickshank, G. D., Tankerville, M. Z., Keswick, B. H., Ellis, B. D., Langworthy, D. E., Metz, K. A., Appleby, M. R., Hamilton, N., Jones, A. L., & Perry, J. D. (2003). Evaluation of a new water treatment for point-of-use household applications to remove microorganisms and arsenic from drinking water. *Journal of Water and Health, 1*(2), 73–84.

Sun, X., & Doner, H. E. (1998). Adsorption and oxidation of arsenite on goethite. *Soil Science, 163*(4), 278–287.

Wang, X., Guo, Y., Yang, L., Han, M., Zhao, J., & Cheng, X. (2012). Nanomaterials as sorbents to remove heavy metal ions in wastewater treatment. *Journal of Environmental Analytical Toxicology, 2*(7), 154(1)–154(7).

Wang, C., Luo, H., Zhang, Z., Wu, Y., Zhang, J., & Chen, S. (2014). Removal of As(III) and As(V) from aqueous solutions using nanoscale zero valent iron-reduced graphite oxide modified composites. *Journal of Hazardous materials, 268*, 124–131.

Weber, W. J., Jr., & Morris, J. C. (1963). Kinetics of adsorption on carbon from solution. *Journal of Sanitation Engineering, Division of American Society Civil Engineering, 89*, 31–60.

WHO. (1993). *Guidelines for drinking water quality Recommendations, 1* (2nd ed.). Geneva: World Health Organization.

Yavuz, C. T., Mayo, J. T., Yu, W. W., Prakash, A., Falkner, J. C., Yean, S., Cong, L., Shipley, H. J., Kan, A., Tomson, M., Natelson, D., & Colvin, V. L. (2006). Low-field magnetic separation of monodisperse Fe₃O₄ nanocrystals. *Science, 314*(5801), 964–967.

Yean, S., Cong, L., Yavuz, C. T., Mayo, J. T., Yu, W. W., Kan, A. T., Colvin, V. L., & Tomson, M. B. (2005). Effect of magnetite particle size on adsorption and desorption of arsenite and arsenate. *Journal of Materials Research, 20*(12), 3255–3264.

Yusof, N. Z., Kassim, M. A., Ismail, R., & Yusoff, A. R. M. (2009). Development of Simple and Cost Effective Method for Arsenic(III) Removal. *Iranica Journal of Energy and Environment, 5*(3), 287–294.

Zhang, Y. M., Yang, M., & Huang, X. (2003). Arsenic (V) removal with a Ce (IV)-doped iron oxide adsorbent. *Chemosphere, 51*(9), 945–952.

Zhao, C., Du, S., Wang, T., Zhang, J., & Luan, Z. (2012). Arsenic removal from drinking water by self-made PMIA nanofiltration membrane. *Advances in Chemical Engineering and Science, 2*(3), 366–371.

Zouboulis, A., & Katsoyiannis, I. (2002). Removal of arsenates from contaminated water by coagulation-direct filtration. *Separation Science and Technology, 37*(12), 2859–2873.